ISSN: 1410-8917
e-ISSN: 2597-9914

Jurnal Kimia Sains dan Aplikasi 27 (8) (2024): 371-380

Jurnal Kimia Sains dan Aplikasi
Journal of Scientific and Applied Chemistry

Journal homepage: http://ejournal.undip.ac.id/index.php/ksa

Synthesis of $NiFe_2O_4$ Magnetic Using *Artocarpus altilis* Leave Extract for Photocatalytic Degradation of Methylene Blue Dye and Antibacterial Applications

Bella Safitri [1], Heni Yohandini [2], Muharni [2], Salni [3], Poedji Loekitowati Hariani [2,*]

[1] Master Program in Chemistry, Faculty of Mathematics and Natural Sciences, Universitas Sriwijaya, Ogan Ilir, Indonesia
[2] Department of Chemistry, Faculty of Mathematics and Natural Sciences, Universitas Sriwijaya, Ogan Ilir, Indonesia
[3] Department of Biology, Faculty of Mathematics and Natural Sciences, Universitas Sriwijaya, Ogan Ilir, Indonesia

* Corresponding author: puji_lukitowati@mipa.unsri.ac.id

https://doi.org/10.14710/jksa.27.8.371-380

Article Info

Article history:

Received: 10th May 2024
Revised: 27th July 2024
Accepted: 16th August 2024
Online: 31st August 2024

Keywords:
Artocapus altilis leave; $NiFe_2O_4$; degradation; methylene blue dye; antibacterial

Abstract

The green synthesis method is an economical and eco-friendly approach to synthesizing materials. This study effectively synthesized magnetic $NiFe_2O_4$ by *Artocarpus altilis* extract leave for the photocatalytic degradation of Methylene blue dye and exhibited antibacterial properties. The phytochemical compounds found in plants act as agents for reducing and stabilizing $NiFe_2O_4$. The synthesized $NiFe_2O_4$ was examined using X-ray diffraction (XRD), scanning electron microscopy with energy-dispersive X-ray spectroscopy (SEM-EDS), ultraviolet-visible diffuse reflectance spectroscopy (UV-DRS), and vibrating sample magnetometry (VSM). The variables in degradation include solution pH, dye concentration, catalyst dose, and irradiation time. The synthesized $NiFe_2O_4$ has a 12.4 nm crystallite size, a saturation magnetization (Ms) of 44.56 emu/g, and a band gap of 1.68 eV. The degradation efficiency of methylene blue dye was 98.2% under the following conditions: a solution pH of 10, a concentration of 10 mg/L, a dose of 0.1 g/L, and an irradiation time of 90 min. The degradation mechanism of Methylene blue dye may be accurately described by pseudo-first-order kinetics, with a k_{app} value of 0.0443 min^{-1}. $NiFe_2O_4$ has high stability; after five degradation cycles, the degradation efficiency decreased by 4.45%. Additionally, $NiFe_2O_4$ demonstrates significant antibacterial activity against *Staphylococcus aureus* and *Escherichia coli* bacteria.

1. Introduction

Organic pollutants, specifically dyes generated by the textile, leather, and printing sectors, are released into surface water and groundwater, posing significant threats to human and ecological health [1, 2]. Around 70% of dye production each year is attributed to azo dyes, which are characterized by the presence of azo groups (– N=N–) as chromophores, along with other functional groups, including sulfonate and hydroxyl groups [3, 4]. Methylene blue dye is extensively utilized in many industrial coloring procedures. Hence, developing efficient, cost-effective, and environmentally friendly methods for treating dye-containing wastewater that does not generate secondary pollutants is important.

Traditional techniques such as chemical oxidation, coagulation, ion exchange, adsorption, and photocatalysis have eliminated dyes [5, 6]. Advanced Oxidation Processes (AOPs) have great potential in decreasing organic and inorganic pollutants. This approach is advantageous due to its cost-effectiveness and environmental sustainability [7]. Among all AOPs techniques, heterogeneous photocatalysis is the most effective in breaking down organic pollutants. When the catalyst absorbs radiation, it produces Reactive Oxygen Species (ROS), which interact with pollutants and break into simpler and non-harmful molecules [8, 9]. Various catalysts, including TiO_2 [10], ZnO [11], SnO_2 [12], and NiO [13], have been extensively employed in the field of photocatalysis. Typically, these oxides possess a

significant band gap (≥3.37 eV) that restricts their ability to convert energy efficiently [14, 15].

The structure of ferrite compounds is represented by the formula MFe_2O_4, where M could refer to Ni, Zn, Fe, Co, or Cu. $NiFe_2O_4$ is considered one of the most important soft materials among ferrite compounds due to its distinctive magnetic and electrical properties. It also exhibits strong chemical stability and mechanical hardness, making it a desirable material for various applications. $NiFe_2O_4$ is a magnetic semiconductor with a low band gap of 1.9 eV that has catalytic properties [6, 16]. Utilizing magnetic $NiFe_2O_4$ for photocatalytic degradation is highly efficient because it can be swiftly and easily separated from the solution after degradation using a permanent magnet without filtering [17].

$NiFe_2O_4$ is utilized in biomedical applications because of its exceptional anisotropy and strong chemical and physical stability. Malik *et al.* [18] demonstrate that $NiFe_2O_4$ exhibits an oxidative stress mechanism that gives rise to its anticancer and antibacterial properties. Other research shows that $NiFe_2O_4$ has antibacterial properties *in vitro* against two bacteria, namely *Pseudomonas aeruginosa* and *Staphylococcus aureus* [16]. The advantageous characteristic of $NiFe_2O_4$ is its capacity to degrade organic pollutants while concurrently impeding the proliferation of pathogenic bacteria.

The synthesis of ferrite compounds can be achieved using numerous techniques, such as solution combustion [17], coprecipitation [19], sol-gel and hydrothermal [20], and microwave radiation [18]. The methods widely used for synthesizing ferrite compounds currently have several drawbacks, including using toxic and expensive chemicals, generating hazardous by-products harmful to the environment, and complex synthesis pathways. Green synthesis is considered a safe and ecologically sound approach [21, 22]. Compared to other methods, the green synthesis method for synthesizing ferrite compounds is plentiful, inexpensive, effective natural resources, and non-toxic and environmentally friendly [23]. Plant extracts and microorganisms, such as fungi and bacteria, are commonly used for the green synthesis of nanoparticles [24].

Phytochemicals are present in several parts of plants, including leaves, flowers, stems, bark, fruit, and roots [25]. The agents involved in the process of biosynthesis are phytochemical molecules that are present in plant extracts, including polyphenols, terpenoids, flavones, polyols, aldehydes, ketones, amides, carboxylic acids, and ascorbic acid. Plants contain proteins, enzymes, and sugars that stabilize nanoparticles and facilitate their interaction with other biomolecules [26]. The phytochemical content in plants is an agent for reducing, complexing, and stabilizing [27]. Various researchers have employed plant extracts to produce ferrite compounds. For instance, Yusefi *et al.* [28] utilized *Garcinia mangostana* fruit peel extract to synthesize Fe_3O_4, Banifatemi *et al.* [29] employed olive leave extract to synthesize $CoFe_2O_4$, and Kattimani *et al.* [30] utilized *Acacia furnesiana* plant for $NiFe_2O_4$ synthesis.

Artocarpus altilis, belonging to the Moraceae family, is commonly known as sukun in Indonesia. This plant is widely distributed in tropical and subtropical regions [31]. Compounds found in the leaves stems, fruits, and bark of breadfruit plants include alkaloids, flavonoids, carbohydrates, terpenoids, tannins, glycosides, steroids, saponins, and carboxylic acids [32]. These compounds are utilized in various biological activities such as antibacterial, anti-tuberculosis, antiviral, antifungal, antiplatelet, anti-arthritis, tyrosinase inhibition, and cytotoxicity [33]. This study investigates the use of *Artocarpus altilis* leaf extract to synthesize $NiFe_2O_4$. *Artocarpus altilis* are readily available in Indonesia, leading to a plentiful supply of raw materials. Besides serving as a photocatalyst for degrading organic pollutants, $NiFe_2O_4$ is also expected to contain antibacterial properties that can eliminate and inhibit the proliferation of microorganisms in the environment.

2. Experimental

2.1. Materials

The materials utilized in this study comprise *Artocarpus altilis* leaves obtained from the Ogan Ilir district, $Fe(NO_3)_3.9H_2O$, $NiNO_3.6H_2O$, methylene blue dye, ethanol, NaOH, HCl and dimethyl sulfoxide (DMSO) produced from Merck, Germany. The microorganisms *S. aureus* and *E. coli* were obtained from PT. Bio Farma.

2.2. *Artocarpus altilis* Leave Extraction

The process began with removing impurities from medium-sized *Artocarpus altilis* leaves and then drying them in the open air for two days. The dried leaves were then pulverized into a fine powder known as simplicia. A total of 100 g of simplicia was immersed in a 96% ethanol solution at a 1:2 ratio. Maceration was conducted for 24 hours with regular stirring every 4 hours. The extract was then separated from the simplicia by filtration, and the concentrated extract was obtained using a rotary evaporator.

2.3. Synthesis of $NiFe_2O_4$

A solution was prepared by dissolving 4.04 g of $Fe(NO_3)_3.9H_2O$ and 1.45 g of $Ni(NO_3)_2.6H_2O$ in 10 mL of distilled water. To this solution, 50 mL of *Artocarpus altilis* leaf extract was added, and the mixture was homogenized for 15 min. The resulting solid was separated from the liquid and subjected to calcination in a furnace at 700°C for 3 hours. The synthesized $NiFe_2O_4$ was then stored in a hermetically sealed container for subsequent characterization and application.

2.4. Characterization of Synthesized $NiFe_2O_4$

The characterization of $NiFe_2O_4$ required the use of a variety of analytical techniques. X-ray diffraction (XRD) (PANalytical, Type: X'Pert PRO) was utilized with a setting of 40 kV and 15 Ma and CuKα λ = 1.5418 Å on the 2θ range of 10-90°. Fourier transform infrared spectroscopy (FTIR) was conducted using a Prestige-21 Shimadzu instrument with KBr pellets. Scanning electron microscopy with energy-dispersive X-ray spectroscopy (SEM-EDX) analysis was utilized to examine the surface morphology and element composition (Thermo Fisher

Scientific Phenom P-Series). Ultraviolet-visible diffuse reflectance spectroscopy (UV-Vis DRS) was carried out using a Cary 60 version type 2.00 instrument. Lastly, magnetic properties were assessed using a vibrating sample magnetometer (VSM) instrument (Quantum design PPMS).

2.5. Determination of pH_{pzc} (Point of Zero Charge)

The solution was prepared by adding 0.02 g of $NiFe_2O_4$ to 0.1 M $NaNO_3$ solution. The pH of the solution was then modified to a pH range from 2 to 12 by utilizing a 0.1 M solution of HCl and NaOH. pH_{pzc} represents where the ΔpH curve ($pH_{initial}$-pH_{final}) intersects with the $pH_{initial}$ axis.

2.6. Photocatalytic Degradation of Methylene Blue Dye

Methylene blue dye was degraded using two 10 W LED lamps with an irradiation intensity of 0.2 mW/cm². The methylene blue dye solution utilized had a volume of 50 mL, and its characteristics included a variable pH range of 2 to 12, a concentration of $NiFe_2O_4$ ranging from 10 to 50 mg/L, and a dosage of $NiFe_2O_4$ ranging from 0.025 to 0.1 g/L. Before the photodegradation process, the mixture was agitated using a magnetic stirrer at a speed of 120 rpm for 30 min under darkness, allowing for the establishment of adsorption-desorption equilibrium. The UV-Vis Spectrophotometer (Orion Aquamate 8000 Type) was used to observe the absorbance of methylene blue dye. Degradation efficiency was calculated using Equation (1).

$$\text{Degradation Efficiency (\%)} = \frac{C_o - C_t}{C_o} x\ 100\ \% \qquad (1)$$

Where, C_o and C_t represent the initial concentration of dye and the concentration of dye at the time.

2.7. Antibacterial Test

The antimicrobial efficacy of $NiFe_2O_4$ was evaluated against two bacterial strains, specifically the Gram-negative bacterium E. coli and the Gram-positive bacterium S. aureus, using the disk diffusion method. A solution of $NiFe_2O_4$ was prepared at 500, 250, 125, 67.5, and 33.75 µg/mL in DMSO solvent and homogenized with a sonicator. Fresh cultures of E. coli and S. aureus were grown to a density of 0.5 McFarland. A 1 mL aliquot of the bacterial suspension was added to a petri dish containing nutrient agar medium and thoroughly mixed. A 0.6 mm-thick paper disc was placed in each petri dish and treated with 10 µL of the $NiFe_2O_4$ solution at varying concentrations. The petri dishes were incubated at 37°C ± 0.1°C for 24 hours, after which the diameter of the inhibition zones was measured. DMSO served as the negative control. The procedure was conducted in triplicate.

3. Results and Discussion

3.1. Characterization of $NiFe_2O_4$

The phytochemicals contained in *Artocarpus altilis* leaf extract have the ability to reduce metal ions and stabilize particles. The mechanism of $NiFe_2O_4$ formation occurs in four stages: metal ion reduction, nucleation, growth, and stabilization. The first step involves the precursor materials, Ni^{2+} and Fe^{3+}, being reduced to Ni^{+}/Ni^{0} and Fe^{2+}/Fe^{0}. Furthermore, the nucleation reaction of $NiFe_2O_4$ occurs through oxidation and the addition of a base. The nucleation process continues to grow into crystals, during which the phytochemicals function as stabilizers to prevent $NiFe_2O_4$ from agglomeration [24, 34]. The mechanism for the synthesis of $NiFe_2O_4$ is shown in Equations (2) and (3).

$$Ni^{2+} + Fe^{3+} + \text{phytochemicals} \rightarrow Ni^{+}/Ni^{0}_{(red)} + Fe^{2+}/Fe^{0}_{(red)} + \text{phytochemicals} \qquad (2)$$

$$Ni^{+}/Ni^{0}_{(red)} + Fe^{2+}/Fe^{0}_{(red)} + \text{phytochemicals} + OH^{-} \rightarrow NiFe_2O_4\text{-phytochemicals} \qquad (3)$$

Figure 1 displays the XRD pattern of $NiFe_2O_4$. The diffraction peak at 2θ belongs to JCPDF No. 54–0964, which exhibits characteristic peaks at specific angles: 30.24°, 35.57°, 37.14°, 45.46°, 47.92°, 53.74°, 57.18°, 62.80°, 66.25°, and 75.30°. These angles correspond to respectively specific crystallographic planes: (220), (311), (222), (400), (411), (422), (511), (440), (531), and (444). The peak observed in the data corresponds to the cubic spinel structure, as elucidated by Bernaoui *et al.* [7]. The lack of further peaks suggests a structure consisting of only one phase [6]. The mean crystallite size of $NiFe_2O_4$ is determined using the Debye-Scherrer equation (Equation (4)).

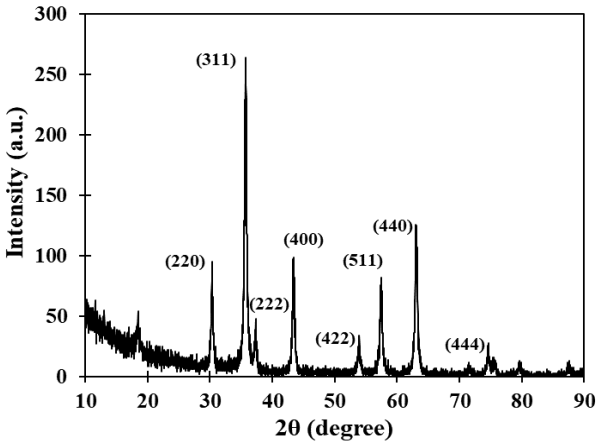

Figure 1. XRD diffraction pattern of $NiFe_2O_4$

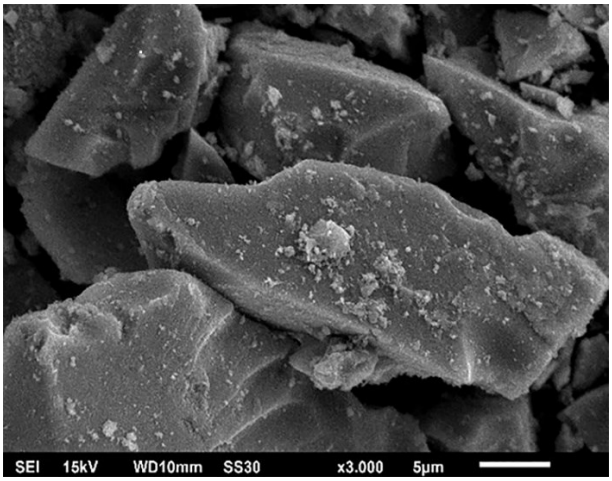

Figure 2. SEM image of $NiFe_2O_4$

$$D = \frac{K\lambda}{\beta \cos\theta} \quad (4)$$

Where D is the crystallite size, K is the Scherrer constant, λ is the X-ray wavelength, β is the full-width half maximum, and θ is the Bragg angle. The crystallite size of $NiFe_2O_4$ is obtained at 12.4 nm. The crystallite size in this study is smaller compared to $NiFe_2O_4$ synthesized using the *Acacia furnesiana* plant, which is 15.5 nm [30]. A smaller crystallite size results in a greater surface area, which enhances catalytic activity.

Figure 2 displays the morphology of $NiFe_2O_4$ at a magnification of 3,000×. The surface of $NiFe_2O_4$ has a spherical shape characterized by varying particle sizes. The EDS analysis results, as shown in Table 1, indicate that the primary constituents of $NiFe_2O_4$ are Ni (21.15%), Fe (42.39%), O (28.68%), and C (7.78%). Element C is derived from the extract of *Artocarpus altilis* leaves.

Figure 3a displays the UV-visible absorbance spectra. $NiFe_2O_4$ exhibits strong absorption in the ultraviolet (UV) and visible spectra. An absorption band was identified at around 750 nm, which is consistent with the observations of Fidelis *et al.* [35] in their synthesis of $NiFe_2O_4$ using the thermal technique. The broad absorption band is attributed to a d-d transition from Ni-36-t2g to Ni-3d-eg [36]. The band gap energy is determined by employing the Tauc equation, which involves calculations based on the Schuster-Kubelka-Munk function (Equation (5)).

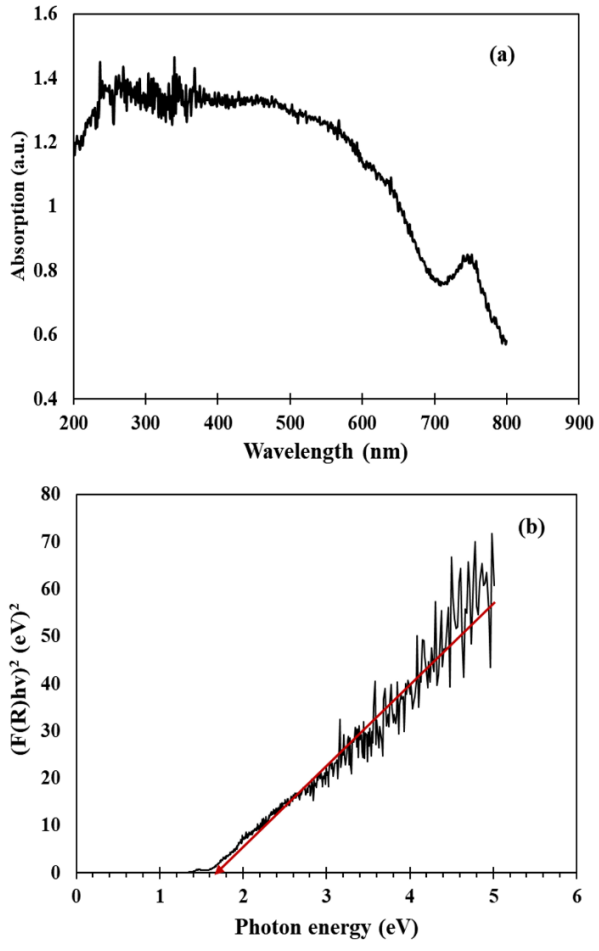

Figure 3. (a) Absorbance spectra and (b) band gap curve of $NiFe_2O_4$

$$F(R).hv = C.(hv - E_g)^n \quad (5)$$

F(R) represents the Schuster-Kubelka-Munk function, directly proportional to the absorption coefficient. The band gap value is determined by extrapolating the square of the product of F(R) and hv against hv at the point where F(R) equals zero [35]. The band gap value of $NiFe_2O_4$ was determined to be 1.68 eV (Figure 3b), which coincides with the value reported by Hemalatha *et al.* [6] for $NiFe_2O_4$ produced via the coprecipitation method.

The magnetic characteristics of $NiFe_2O_4$ were analyzed using a VSM at normal ambient temperature (Figure 4). The research findings indicated that the magnetic saturation (MS) value measured 46.80 emu/g. In contrast to the study conducted by Abbas *et al.* [37], the MS value of $NiFe_2O_4$ synthesized by the co-precipitation approach was 32.9 emu/g, while $NiFe_2O_4$ synthesized using *Murayya koenigii* extract had an MS value of 5.2 emu/g [38]. The MS value of the material is lower than that of bulk $NiFe_2O_4$, which is 55 emu/g, according to Rincón-Granados *et al.* [16]. The application of a non-magnetic coating made from *Artocarpus altilis* leave extract decreases the magnetic characteristics.

3.2. Photocatalytic Degradation of Methylene Blue Dye

The pH of the solution heavily influences the degradation process. The degradation process begins with the adsorption of dye molecules onto the surface of the catalyst [39]. The affinity between the dye and $NiFe_2O_4$ governs the interaction. In an acidic solution, there is competition between H^+ ions and methylene blue dye, which is positively charged (cationic dye), for attraction to the $NiFe_2O_4$ surface. The pH_{pzc} of $NiFe_2O_4$ was determined to be 7.2, as shown in Figure 5a. When the pH is higher than the pH_{pzc}, $NiFe_2O_4$ has a negative charge. As a result, a higher pH leads to more breakdown because of the attractive forces between the positively charged dye and the negatively charged $NiFe_2O_4$. The study found that the highest level of degradation occurred at a pH of 10, resulting in a reduction of 78.56% (Figure 5b). Additional studies indicate that the most favorable pH range for the breakdown of methylene blue dye is in alkaline conditions, specifically between pH 9 and 12 [39, 40]. The degrading mechanism was described [21] in Equations (5) to (8).

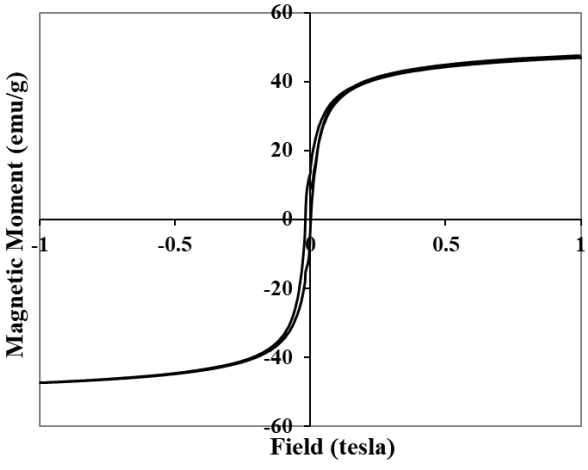

Figure 4. The magnetization curve of $NiFe_2O_4$ composite

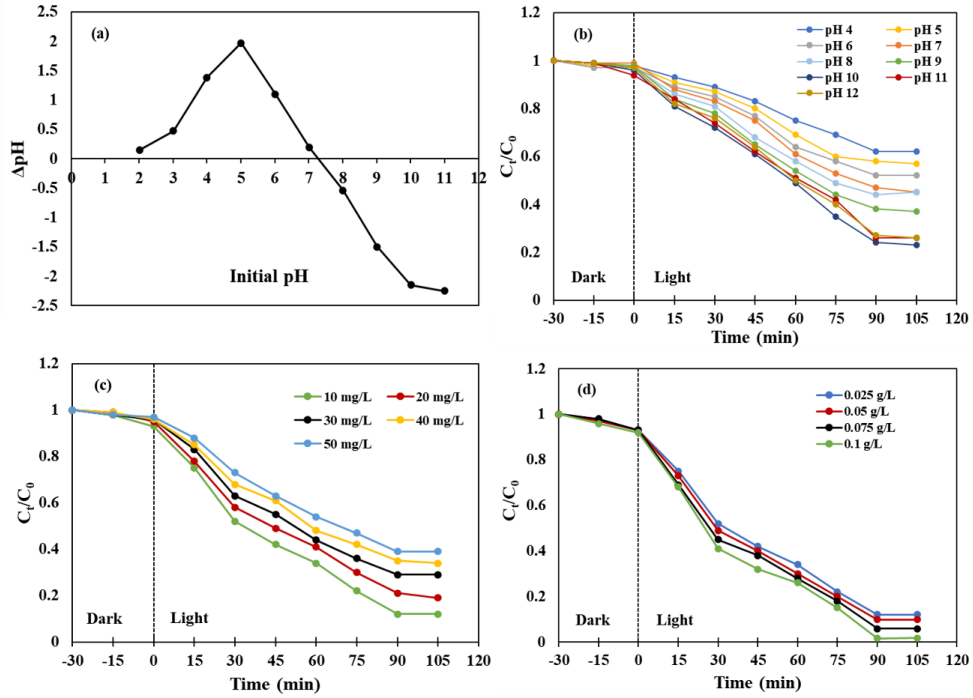

Figure 5. (a) pH_{pzc}, and effect of (b) pH solution, (c) methylene blue dye concentration, and (d) irradiation time to the C_t/C_0

$$NiFe_2O_4 + hv \rightarrow NiFe_2O_4 + (e_{CB}^- + h_{VB}^+) \quad (5)$$

$$NiFe_2O_4 + (e_{CB}^-) + O_2 \rightarrow (\cdot O_2^-) \quad (6)$$

$$NiFe_2O_4 + (h_{VB}^+) + H_2O \rightarrow NiFe_2O_4 + H^+ + \cdot OH \quad (7)$$

$$MB + \cdot O_2^- + \cdot OH \rightarrow CO_2 + H_2O + \text{other product} \quad (8)$$

When $NiFe_2O_4$ is exposed to irradiation, electrons are stimulated from the lower Valence Band (VB) energy level to the higher Conduction Band (CB) energy level, leading to the creation of vacancies in the VB. The hole in VB reacts with water to form hydroxyl radicals (·OH). Concurrently, oxygen molecules that are dissolved on the surface of $NiFe_2O_4$ nanoparticles engage with electrons on CB, forming superoxide radicals ($\cdot O_2^-$). Reactive species on the $NiFe_2O_4$ surface act as a potent oxidizing agent, leading to the degradation of the methylene blue dye on the catalyst surface. The mineralization process by reactive species produces CO_2 and H_2O molecules [17, 41].

Figure 5(c) illustrates a negative correlation between the concentration of methylene blue dye and its degradation efficiency. The degradation efficiency was 88.4% when the concentration of methylene blue dye was 10 mg/L, but it reduced to 61.6% when the concentration was increased to 50 mg/L. Abd El Khalk *et al.* [39] observed the same behavior when degrading methylene blue dye with a zeolitic imidazolate nanocomposite. At elevated concentrations of methylene blue dye, there is an increase in the adsorption of dye on the surface of the photocatalyst. This hinders light penetration on the catalyst surface, resulting in insufficient reactive species for the degradation process [38].

Optimizing degradation requires careful consideration of catalyst dose. The dose variations in this investigation ranged from 0.025 to 0.1 g/L, with increments of 0.025 g/L. The degradation efficiency using a catalyst dose of 0.025 g/L was 88.4%, with a methylene blue dye concentration of 10 mg/L and 90 min irradiation time. Augmenting the amount of catalyst leads to a corresponding enhancement in degradation efficiency. The highest degradation efficiency was achieved at a concentration of 0.1 g/L, resulting in a degradation efficiency of 98.2% (Figure 5d). Increasing the catalyst dosage leads to a more significant number of active sites available for degrading methylene blue dye, improving degradation efficiency [42, 43].

3.3. Kinetics Studies

The photodegradation rate of methylene blue dye using $NiFe_2O_4$ in this study was tested using a pseudo-first-order equation (Equation (9)) [44].

$$Ln\, {}^{C}/_{C_0} = -k_{app}t \quad (9)$$

Where, C and C_0 represent the concentrations at time t and t = 0, respectively, while k_{app} denotes a pseudo-first-order constant. The concentration of methylene blue dye used was 10 mg/L, the pH of the solution was 10, and the catalyst dose was 0.1 g/L (Figure 6). The obtained R^2 value was 0.993, which is close to 1, indicating a high level of linearity [21]. The obtained value for k_{app} is 0.0443 min^{-1}. Degradation of methylene blue dye initially proceeded slowly and then increased rapidly. The slow phase is termed the induction period, during which the methylene blue dye remains on the surface of the catalyst [7]. The k_{app} value exceeds the degradation rate of methylene blue dye employing CdS Nanorods at the same pH (pH 10), namely 0.0391 min^{-1} [45].

Table 1 presents a comparative analysis of the degradation of methylene blue dye utilizing other materials. The study demonstrates that the degradation efficiency of methylene blue dye using $NiFe_2O_4$ is superior to that of other methods.

Table 1. Degradation of methylene blue dye by some materials

Material	Dye concentration (mg/L)	Catalyst dose (g/L)	Irradiation time (min)	Degradation efficiency (%)	Ref.
$ZnFe_2O_4@SiO_2@TiO_2$	10	1.0	120	95.1	[46]
CuO/Bi_2O_3	10	0.2	120	87.8	[47]
TiO_2-MoO_3	12.6	0.33	210	33.0	[48]
TiO_2/g-C_3N_5	20	-	105	92.4	[49]
$CuNiFe_2O_4/g$-C_3N_4	15	0.8	180	97.23	[50]
CeO_2-NPs/graphene oxide/polyacrylamide	5	0.25	90	90.0	[40]
$NiFe_2O_4/ZnO$	5	0.05	130	91.36	[51]
CuO	5	0.2	60	97.0	[43]
$NiFe_2O_4$	10	0.1	90	98.2	This work

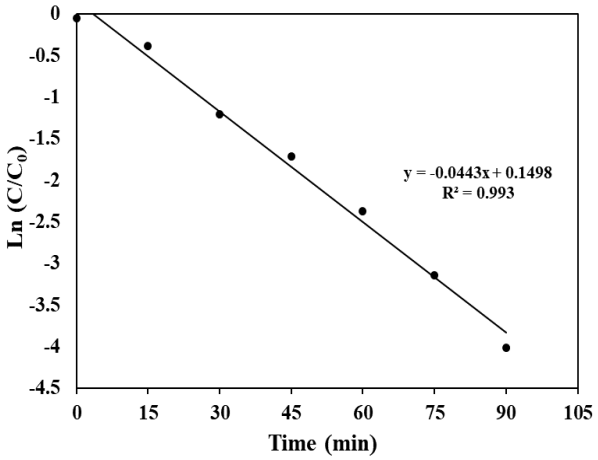

Figure 6. Kinetics model of $NiFe_2O_4$ for methylene blue dye degradation

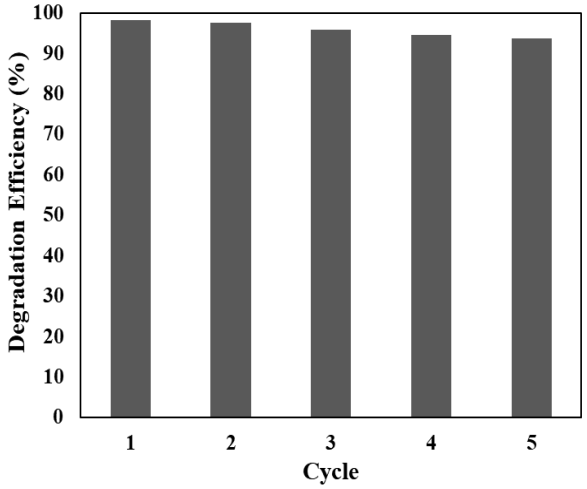

Figure 7. Recycle efficiency of $NiFe_2O_4$ for methylene blue dye degradation

3.4. Recyclability of Catalysts

Photocatalyst stability and recyclability are crucial when considering catalysts in various applications [43]. Catalyst recyclability assessment is achieved by submitting the composite to degradation processes. The method begins with an external magnet separating the catalyst from the mixture, followed by the degradation process, which is washed repeatedly with distilled water and ethanol. The catalyst was dried at 80°C for 5 h before being utilized again [19]. Figure 7 demonstrates that employing a catalyst for 5 cycles reduced degradation efficiency by 4.45%. The degradation efficiency for five cycles was 98.20%, 97.60%, 95.85%, 94.40%, and 93.75%. The results suggest that the stable catalyst can be employed multiple times, making it suitable for industrial applications in liquid waste treatment.

3.5. Effect of Scavenger

Scavenger analysis is employed to evaluate the active radicals produced during photodegradation. The findings depicted in Figure 8 indicate that the degradation efficiency of methylene blue dye is impacted by various factors, including a 90-minute irradiation time, a dye concentration of 10 mg/L, and a catalyst dose of 0.1 g/L. In terms of effectiveness, ranked from highest to lowest, H_2O_2, disodium ethylene diamine tetraacetate (EDTA), and isopropyl alcohol (IPA) are observed. The superior efficacy of H_2O_2 is primarily attributed to the generation of hydroxyl radicals [6]. EDTA and IPA led to a noticeable decrease in photodegradation efficiency, affirming the substantial involvement of H^+ and ·OH radicals in the photodegradation process [52].

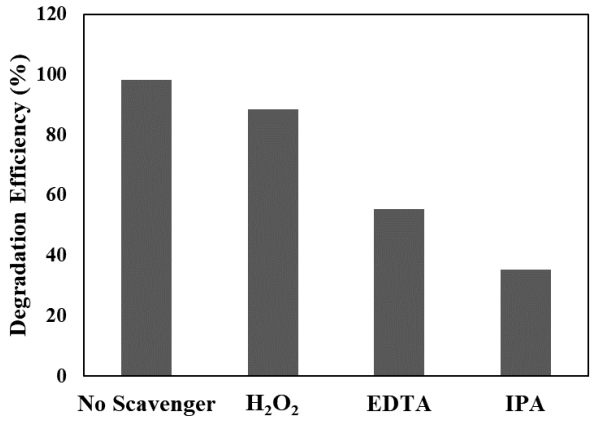

Figure 8. The effect of scavenger for methylene blue dye degradation

3.6. Antibacterial Activity

The antibacterial activity test was conducted on two types of bacteria, specifically *S. aureus* and *E. coli*. The values of $NiFe_2O_4$ ranged from 500 µg/mL to 33.75 µg/mL. Table 2 displays the inhibitory values for each microorganism. The size of the inhibition zone expands as the concentration of $NiFe_2O_4$ increases. The minimum inhibitory concentrations (MIC) of 67.5 µg/mL exhibited potent activity against both *S. aureus* and *E. coli* bacteria, resulting in inhibition zones of 13.2 mm and 10.2 mm, respectively. The findings indicated that the growth inhibition zone for *S. aureus* bacteria surpassed that of *E. coli*. The vulnerability of *E. coli* bacteria compared to *S. aureus* is due to a substantial peptidoglycan coating in the walls of gram-positive bacteria [41]. A similar result was obtained when the synthesis of $NiFe_2O_4$ using lime peel extract indicated that the inhibitory zone for *E. coli* bacteria was smaller than that of *S. aureus* bacteria. At a concentration of $NiFe_2O_4$ of 50 µg/mL, the inhibition zones against *E. coli* and *S. aureus* are around 13 mm and 14 mm, respectively [18].

The antibacterial activity is achieved by various processes, including liberating toxic ions (Ni^{2+} and Fe^{3+}) that can infiltrate bacterial cells, oxidative stress, mechanical disruption of membranes, enzymatic inhibition, and proteolysis [53]. Other research indicates that $NiFe_2O_4$ can hinder the proliferation of several bacteria, including *S. aureus, E. coli, Staphylococcus epidermis, Staphylococcus xylosus, Staphylococcus saprophyticus,* and *Pseudomonas aeruginosa* [38].

Table 2. Zone of inhibition of $NiFe_2O_4$

Concentration (µg/mL)	Inhibition zone (mm)	
	S. aureus	*E. coli*
500	22.4 ± 0.28	19.5 ± 0.35
250	18.2 ± 0.09	17.8 ± 0.22
125	15.4 ± 0.11	13.6 ± 0.21
67.5	13.2 ± 0.08	10.2 ± 0.45
33.75	0	0
(-)	0	0

4. Conclusion

The green synthesis method, mainly using *Artocarpus altilis* leave extract, has been effectively employed to produce $NiFe_2O_4$ with magnetic characteristics. $NiFe_2O_4$ degrades methylene blue dye with 98.2% efficiency when exposed to visible light at a solution pH of 10, Methylene blue dye concentration of 10 mg/L, dose of 0.1 g/L, and irradiation time of 90 min. The magnetic characteristics of $NiFe_2O_4$ are crucial for the catalyst's recyclability and reusability. The catalyst has excellent stability, as it may be reused for up to 5 cycles without any notable loss in degradation efficiency (4.45%). The results indicate that the $NiFe_2O_4$ catalyst demonstrates proficiency in degrading Methylene blue dye and exhibits antibacterial properties against gram-positive and gram-negative bacteria, particularly *S. aureus* and *E. coli*. Consequently, it holds potential for wastewater treatment applications.

Acknowledgment

The research was supported by a grant awarded (Hibah Profesi) Universitas Sriwijaya with contract number 0187/UN9.3.1/SK/2023 on April 18, 2023.

References

[1] Lemya Boughrara, Farouk Zaoui, M'hamed Guezzoul, Fatima Zohra Sebba, Boumediene Bounaceur, Seghier Ould Kada, New alginic acid derivatives ester for methylene blue dye adsorption: kinetic, isotherm, thermodynamic, and mechanism study, *International Journal of Biological Macromolecules*, 205, (2022), 651-663 https://doi.org/10.1016/j.ijbiomac.2022.02.087

[2] Somia Djelloul Bencherif, Juan Jesús Gallardo, Iván Carrillo-Berdugo, Abdellah Bahmani, Javier Navas, Synthesis, Characterization and Photocatalytic Performance of Calcined ZnCr-Layered Double Hydroxides, *Nanomaterials*, 11, 11, (2021), 3051 https://doi.org/10.3390/nano11113051

[3] Liping Sun, Yinghui Mo, Lu Zhang, A mini review on bio-electrochemical systems for the treatment of azo dye wastewater: State-of-the-art and future prospects, *Chemosphere*, 294, (2022), 133801 https://doi.org/10.1016/j.chemosphere.2022.133801

[4] Lukman A. Yusuf, Zeliha Ertekin, Shaun Fletcher, Mark D. Symes, Enhanced ultrasonic degradation of methylene blue using a catalyst-free dual-frequency treatment, *Ultrasonics Sonochemistry*, 103, (2024), 106792 https://doi.org/10.1016/j.ultsonch.2024.106792

[5] Zuming He, Yongmei Xia, Jiangbin Su, Bin Tang, Fabrication of magnetically separable $NiFe_2O_4/Bi_{24}O_{31}Br_{10}$ nanocomposites and excellent photocatalytic performance under visible light irradiation, *Optical Materials*, 88, (2019), 195-203 https://doi.org/10.1016/j.optmat.2018.11.025

[6] J. Hemalatha, M. Senthil, D. Madhan, Amal M. Al-Mohaimeed, Wedad A. Al-onazi, Fabrication of $NiFe_2O_4$ nanoparticles loaded on activated carbon as novel composites for high efficient ultra violet-light photocatalysis for degradation of aqueous organic pollutants, *Diamond and Related Materials*, 144, (2024), 110995 https://doi.org/10.1016/j.diamond.2024.110995

[7] Cheikh Reda Bernaoui, Abdelaziz Bendraoua, Farouk Zaoui, Juan Jesús Gallardo, Javier Navas, Rafik Abdelkrim Boudia, Houria Djediai, Nor el Houda Goual, Mehdi Adjdir, Synthesis and characterization of $NiFe_2O_4$ nanoparticles as reusable magnetic nanocatalyst for organic dyes catalytic reduction: Study of the counter anion effect, *Materials Chemistry and Physics*, 292, (2022), 126793 https://doi.org/10.1016/j.matchemphys.2022.126793

[8] Fatima Habeche, Mohammed Hachemaoui, Adel Mokhtar, Karim Chikh, Fadila Benali, Amel Mekki, Farouk Zaoui, Zakaria Cherifi, Bouhadjar Boukoussa, Recent Advances on the Preparation and Catalytic Applications of Metal Complexes Supported-Mesoporous Silica MCM-41 (Review), *Journal of Inorganic and Organometallic Polymers and Materials*, 30, 11, (2020), 4245-4268 https://doi.org/10.1007/s10904-020-01689-1

[9] Dan Feng, Audrey Soric, Olivier Boutin, Treatment technologies and degradation pathways of glyphosate: A critical review, *Science of The Total Environment*, 742, (2020), 140559 https://doi.org/10.1016/j.scitotenv.2020.140559

[10] Rahmat Hidayat, Ganjar Fadillah, Shin-Ichi Ohira, Febi Indah Fajarwati, Dian Ayu Setyorini, Anggi Saputra, Facile green synthesis of Ag doped TiO_2 nanoparticles using maple leaf for bisphenol-A degradation and its antibacterial properties, *Materials Today Sustainability*, 26, (2024), 100752 https://doi.org/10.1016/j.mtsust.2024.100752

[11] Md Abdulla Sayem, Md Amran Hossen Suvo, Ishtiaque M. Syed, Mahabub Alam Bhuiyan, Effective adsorption and visible light driven enhanced photocatalytic degradation of rhodamine B using ZnO nanoparticles immobilized on graphene oxide nanosheets, *Results in Physics*, 58, (2024), 107471 https://doi.org/10.1016/j.rinp.2024.107471

[12] P. A. Luque, H. E. Garrafa-Gálvez, O. Nava, A. Olivas, M. E. Martínez-Rosas, A. R. Vilchis-Nestor, A. Villegas-Fuentes, M. J. Chinchillas-Chinchillas, Efficient sunlight and UV photocatalytic degradation of Methyl Orange, Methylene Blue and Rhodamine B, using *Citrus×paradisi* synthesized SnO_2 semiconductor nanoparticles, *Ceramics International*, 47, 17, (2021), 23861-23874 https://doi.org/10.1016/j.ceramint.2021.05.094

[13] Kathirvel Brindhadevi, T. P. Kim, Sulaiman Ali Alharbi, M. D. Ramesh, Jintae Lee, Devaraj Bharathi, Enhanced photocatalytic degradation of polycyclic aromatic hydrocarbons (PAHs) Using NiO nanoparticles, *Environmental Research*, 252, (2024), 118454 https://doi.org/10.1016/j.envres.2024.118454

[14] Seerangaraj Vasantharaj, Selvam Sathiyavimal, Palanisamy Senthilkumar, Felix LewisOscar, Arivalagan Pugazhendhi, Biosynthesis of iron oxide nanoparticles using leaf extract of *Ruellia tuberosa*: Antimicrobial properties and their applications in photocatalytic degradation, *Journal of Photochemistry and Photobiology B: Biology*, 192, (2019), 74-82 https://doi.org/10.1016/j.jphotobiol.2018.12.025

[15] Keerti Jain, Anand S. Patel, Vishwas P. Pardhi, Swaran Jeet Singh Flora, Nanotechnology in Wastewater Management: A New Paradigm Towards Wastewater Treatment, *Molecules*, 26, 6, (2021), 1797 https://doi.org/10.3390/molecules26061797

[16] Karen L. Rincón-Granados, América R. Vázquez-Olmos, Adriana-Patricia Rodríguez-Hernández, Alejandro Vega-Jiménez, Fabián Ruiz, Vicente Garibay-Febles, Laurie-Ann Ximénez-Fyvie, Facile solid-state synthesis and study in vitro of the antibacterial activity of NiO and $NiFe_2O_4$ nanoparticles, *Materialia*, 15, (2021), 100955 https://doi.org/10.1016/j.mtla.2020.100955

[17] Poedji Loekitowati Hariani, Muhammad Said, Addy Rachmat, Fahma Riyanti, Handayani Citra Pratiwi, Widya Twiny Rizki, Preparation of $NiFe_2O_4$ Nanoparticles by Solution Combustion Method as Photocatalyst of Congo red, *Bulletin of Chemical Reaction Engineering & Catalysis*, 16, 3, (2021), 481-490 https://doi.org/10.9767/bcrec.16.3.10848.481-490

[18] Abdul Raouf Malik, Muhammad Hammad Aziz, Muhammad Atif, Muhammad Sultan Irshad, Hafeez Ullah, Tuan Nguyen Gia, Hijaz Ahmed, Shafiq Ahmad, Thongchai Botmart, Lime peel extract induced $NiFe_2O_4$ NPs: Synthesis to applications and oxidative stress mechanism for anticancer, antibiotic activity, *Journal of Saudi Chemical Society*, 26, 2, (2022), 101422 https://doi.org/10.1016/j.jscs.2022.101422

[19] Trimurti L. Lambat, Pankaj V. Ledade, Jitendra K. Gunjate, Vivek R. Bahekar, Sami H. Mahmood, Subhash Banerjee, Recent developments in the organic synthesis using nano-$NiFe_2O_4$ as reusable catalyst: A comprehensive synthetic & catalytic reusability protocol, *Results in Chemistry*, 6, (2023), 101176 https://doi.org/10.1016/j.rechem.2023.101176

[20] Farzana Majid, Javeria Rauf, Sadia Ata, Ismat Bibi, Abdul Malik, Sobhy M. Ibrahim, Adnan Ali, Munawar Iqbal, Synthesis and characterization of $NiFe_2O_4$ ferrite: Sol–gel and hydrothermal synthesis routes effect on magnetic, structural and dielectric characteristics, *Materials Chemistry and Physics*, 258, (2021), 123888 https://doi.org/10.1016/j.matchemphys.2020.123888

[21] Yilin Liu, Tong Liu, Linfeng Zhang, Huadong Wu, Jia Guo, Xuelei Hu, One-pot synthesized $NiFe_2O_4/CeO_2$ composite catalyst for efficient degradation of methylene blue via photocatalysis under visible light, *Catalysis Communications*, 185, (2023), 106814 https://doi.org/10.1016/j.catcom.2023.106814

[22] Rajender S. Varma, Greener approach to nanomaterials and their sustainable applications, *Current Opinion in Chemical Engineering*, 1, 2, (2012), 123-128 https://doi.org/10.1016/j.coche.2011.12.002

[23] Salar Hafez Ghoran, Maryam Fadaei Dashti, Aram Maroofi, Mustafa Shafiee, Alireza Zare-Hoseinabadi, Farahnaz Behzad, Mohsen Mehrabi, Ali Jangjou, Kazem Jamali, Biosynthesis of Zinc Ferrite Nanoparticles Using Polyphenol-rich extract of Citrus aurantium flowers, *Nanomedicine Research Journal*, 5, 1, (2020), 20-28 https://doi.org/10.22034/NMRJ.2020.01.003

[24] Dyah Ayu Larasati, Deska Lismawenning Puspitarum, Mahardika Yoga Darmawan, Nurul Imani Istiqomah, Juliasih Partini, Hasniah Aliah, Edi Suharyadi, Green synthesis of $CoFe_2O_4$/ZnS composite nanoparticles utilizing *Moringa Oleifera* for magnetic hyperthermia applications, *Results in Materials*, 19, (2023), 100431 https://doi.org/10.1016/j.rinma.2023.100431

[25] Yunhui Bao, Jian He, Ke Song, Jie Guo, Xianwu Zhou, Shima Liu, Plant-Extract-Mediated Synthesis of Metal Nanoparticles, *Journal of Chemistry*, 2021, 1, (2021), 6562687 https://doi.org/10.1155/2021/6562687

[26] Imtiyaz Hussain, N. B. Singh, Ajey Singh, Himani Singh, S. C. Singh, Green synthesis of nanoparticles and its potential application, *Biotechnology Letters*, 38, 4, (2016), 545-560 https://doi.org/10.1007/s10529-015-2026-7

[27] Thana Shuga Aldeen, Hamza Elsayed Ahmed Mohamed, Malik Maaza, ZnO nanoparticles prepared via a green synthesis approach: Physical properties, photocatalytic and antibacterial activity, *Journal of Physics and Chemistry of Solids*, 160, (2022), 110313 https://doi.org/10.1016/j.jpcs.2021.110313

[28] Mostafa Yusefi, Kamyar Shameli, Ong Su Yee, Sin-Yeang Teow, Ziba Hedayatnasab, Hossein Jahangirian, Thomas J. Webster, Kamil Kuča, Green synthesis of Fe_3O_4 nanoparticles stabilized by a *Garcinia mangostana* fruit peel extract for hyperthermia and anticancer activities, *International Journal of Nanomedicine*, 2021, 16, (2021), 2515-2532 https://doi.org/10.2147/IJN.S284134

[29] S. S. Banifatemi, F. Davar, B. Aghabarari, Juan A. Segura, Francisco J. Alonso, Seyyed M. Ghoreishi, Green synthesis of $CoFe_2O_4$ nanoparticles using olive leaf extract and characterization of their magnetic properties, *Ceramics International*, 47, 13, (2021), 19198-19204 https://doi.org/10.1016/j.ceramint.2021.03.267

[30] Veeranna R. Kattimani, K. V. Yatish, K. Pramoda, M. Sakar, R. Geetha Balakrishna, *Acacia furnesiana* plant as a novel green source for the synthesis of $NiFe_2O_4$ magnetic nanocatalyst and as feedstock for sustainable high quality biofuel production, *Fuel*, 348, (2023), 128549 https://doi.org/10.1016/j.fuel.2023.128549

[31] Mukesh S. Sikarwar, Boey Jia Hui, Kumutha Subramaniam, Bavani Devi Valeisamy, Ling Kar Yean, Kaveti Balaji, A Review on *Artocarpus altilis* (Parkinson) Fosberg (breadfruit), *Journal of Applied Pharmaceutical Science*, 4, 8, (2014), 091-097

[32] Carmen X. Luzuriaga-Quichimbo, José Blanco-Salas, Carlos E. Cerón-Martínez, Trinidad Ruiz-Téllez, Providing added value to local uses of paparahua (*Artocarpus altilis*) in Amazonian Ecuador by phytochemical data review, *Revista Brasileira de Farmacognosia*, 29, 1, (2019), 62-68 https://doi.org/10.1016/j.bjp.2018.09.008

[33] U. B. Jagtap, V. A. Bapat, Artocarpus: A review of its traditional uses, phytochemistry and pharmacology, *Journal of Ethnopharmacology*, 129, 2, (2010), 142-166 https://doi.org/10.1016/j.jep.2010.03.031

[34] Lisha Liu, Yuanhua Li, Arwa A. Al-Huqail, Elimam Ali, Tamim Alkhalifah, Fahad Alturise, H. Elhosiny Ali, Green synthesis of Fe_3O_4 nanoparticles using Alliaceae waste (Allium sativum) for a sustainable landscape enhancement using support vector regression, *Chemosphere*, 334, (2023), 138638 https://doi.org/10.1016/j.chemosphere.2023.138638

[35] Michel Zampieri Fidelis, Giulia Caroline de Cristo Borges, Eduardo Abreu, Giane Gonçalves Lenzi, Henrique Emilio Zorel Junior, Odivaldo Cambraia Alves, Rodrigo Brackmann, Onelia Aparecida Bassoli Andreo, $NiFe_2O_4$–TiO_2 magnetic nanoparticles synthesized by the thermal decomposition of 8-hydroxyquinolinates as efficient photocatalysts for the removal of As(III) from water, *Optical Materials*, 145, (2023), 114490 https://doi.org/10.1016/j.optmat.2023.114490

[36] Subrata Karmakar, Krutika L. Routray, Bandana Panda, Bibekananda Sahoo, Dhrubananda Behera, Construction of core@shell nanostructured $NiFe_2O_4$@TiO_2 ferrite NAND logic gate using fluorescence quenching mechanism for TiO_2 sensing, *Journal of Alloys and Compounds*, 765, (2018), 527-537 https://doi.org/10.1016/j.jallcom.2018.06.100

[37] Zena Mohammed Ali Abbas, Wafaa A. Shatti, Mahmood M. Kareem, Ziad T. Khodair, Synthesis and characterization of $NiFe_2O_4$/CuO nanocomposites: Structural and magnetic properties analysis, *Chemical Data Collections*, 47, (2023), 101078 https://doi.org/10.1016/j.cdc.2023.101078

[38] Waleed M. Alamier, Nazim Hasan, M. D. Sarfaraz Nawaz, Khatib Sayeed Ismail, Mohd Shkir, Maqsood Ahmad Malik, Mohammed D. Y. Oteef, Biosynthesis of $NiFe_2O_4$ nanoparticles using *Murayya koenigii* for photocatalytic dye degradation and antibacterial application, *Journal of Materials Research and Technology*, 22, (2023), 1331-1348 https://doi.org/10.1016/j.jmrt.2022.11.181

[39] Amira Ahmed Abd El Khalk, Mohamed Ahmed Betiha, Ahmed Sadek Mansour, Mohamed Gamal Abd El Wahed, Ahmad Mohamad Al-Sabagh, High Degradation of Methylene Blue Using a New Nanocomposite Based on Zeolitic Imidazolate Framework-8, *ACS Omega*, 6, 40, (2021), 26210-26220 https://doi.org/10.1021/acsomega.1c03195

[40] Zeynep Kalaycıoğlu, Bengü Özuğur Uysal, Önder Pekcan, F. Bedia Erim, Efficient Photocatalytic Degradation of Methylene Blue Dye from Aqueous Solution with Cerium Oxide Nanoparticles and Graphene Oxide-Doped Polyacrylamide, *ACS Omega*, 8, 14, (2023), 13004-13015 https://doi.org/10.1021/acsomega.3c00198

[41] Aubrey Makofane, Popoti J. Maake, Morongwa M. Mathipa, Nolubabalo Matinise, Franscious R. Cummings, David E. Motaung, Nomso C. Hintsho-Mbita, Green synthesis of $NiFe_2O_4$ nanoparticles for the degradation of Methylene Blue, sulfisoxazole and bacterial strains, *Inorganic Chemistry Communications*, 139, (2022), 109348 https://doi.org/10.1016/j.inoche.2022.109348

[42] Yixing Gao, Wenping Cao, Kaixuan Wang, Hangyu Shi, Shumin Wang, Qingnan Meng, Keqin Du, Chuan Wang, Junliang Lin, Performance and mechanism of magnetic Fe_3O_4@MnO_2 catalyst for rapid degradation of methylene blue by activation of peroxymonosulfate, *Journal of Alloys and Compounds*, 987, (2024), 174144 https://doi.org/10.1016/j.jallcom.2024.174144

[43] M. MuthuKathija, Selvaraj Muthusamy, R. Imran Khan, M. Sheik Muhideen Badhusha, Kanagaraj Rajalakshmi, V. Rama, Yuanguo Xu, Photocatalytic degradation of methylene blue dye using biogenic copper oxide nanoparticles and its degradation pathway analysis, *Inorganic Chemistry Communications*, 161, (2024), 111929 https://doi.org/10.1016/j.inoche.2023.111929

[44] Vijayamari Arumugaperumal, Sadaiyandi K., Solar light driven photocatalytic degradation of methylene blue dye over Cu doped α -MnO_2 nanoparticles, *Chemical Physics Impact*, 8, (2024), 100434 https://doi.org/10.1016/j.chphi.2023.100434

[45] Sook-Keng Chang, Qurat-ul-Ain Abbasi, Zeeshan Abbasi, Fatima Khushbakht, Inam Ullah, Fazal Ur Rehman, Muhammad Hafeez, Rapid pH-dependent Photocatalytic Degradation of Methylene Blue by CdS Nanorods Synthesized through Hydrothermal Process, *Arabian Journal of Chemistry*, 17, 1, (2024), 105422 https://doi.org/10.1016/j.arabjc.2023.105422

[46] Xianfeng Meng, Yan Zhuang, Hua Tang, Chunhua Lu, Hierarchical structured $ZnFe_2O_4$@SiO_2@TiO_2 composite for enhanced visible-light photocatalytic activity, *Journal of Alloys and Compounds*, 761, (2018), 15-23 https://doi.org/10.1016/j.jallcom.2018.05.150

[47] Fatemeh Poorsajadi, Mohammad Hossein Sayadi, Mahmood Hajiani, Mohammad Reza Rezaei, Synthesis of CuO/Bi_2O_3 nanocomposite for efficient and recycling photodegradation of methylene blue dye, *International Journal of Environmental Analytical Chemistry*, 102, 18, (2022), 7165-7178 https://doi.org/10.1080/03067319.2020.1826464

[48] Vincent Otieno Odhiambo, Thong Le Ba, Zoltán Kónya, Csaba Cserháti, Zoltán Erdélyi, Maritim C Naomi, Imre Miklós Szilágyi, Preparation of TiO_2–MoO_3 composite nanofibers by water-based electrospinning process and their application in photocatalysis, *Materials Science in Semiconductor Processing*, 147, (2022), 106699 https://doi.org/10.1016/j.mssp.2022.106699

[49] Yuan Zhang, Tianyi Cui, Jianbo Zhao, Yumin Yan, Jianhui Jiang, Fabrication and study of a novel TiO_2/g-C_3N_5 material and photocatalytic properties using methylene blue and tetracycline under visible light, *Inorganic Chemistry Communications*, 143, (2022), 109815 https://doi.org/10.1016/j.inoche.2022.109815

[50] Ibrahim F. Waheed, Muwafaq A. Hamad, Khalaf A. Jasim, Andre J. Gesquiere, Degradation of methylene blue using a novel magnetic $CuNiFe_2O_4$/g-C_3N_4 nanocomposite as heterojunction photocatalyst, *Diamond and Related Materials*, 133, (2023), 109716 https://doi.org/10.1016/j.diamond.2023.109716

[51] Tripta, Pawan S. Rana, $NiFe_2O_4$/ZnO nanocomposites for degradation of MB dye with their local electrical behavior, *Journal of Molecular Structure*, 1282, (2023), 135160 https://doi.org/10.1016/j.molstruc.2023.135160

[52] Nan Wang, Juan Li, Lyumeng Ye, Xinjun Li, Heterogeneous nanostructure anatase/rutile titania supported platinum nanoparticles for efficient photocatalytic degradation of methylene blue dyes, *Sustainable Chemistry for the Environment*, 5, (2024), 100072 https://doi.org/10.1016/j.scenv.2024.100072

[53] A. Manohar, V. Vijayakanth, Ruoyu Hong, Solvothermal reflux synthesis of $NiFe_2O_4$ nanocrystals dielectric and magnetic hyperthermia properties, *Journal of Materials Science: Materials in Electronics*, 31, 1, (2020), 799-806 https://doi.org/10.1007/s10854-019-02588-z